IEEE Access
Multidisciplinary | Rapid Review | Open Access Journal

Received June 14, 2019, accepted July 19, 2019, date of publication July 25, 2019, date of current version August 9, 2019.

Digital Object Identifier 10.1109/ACCESS.2019.2931087

Optimized Radar Waveform Parameter Design for Small Drone Detection Based on Echo Modeling and Experimental Analysis

TENGMINGYANG LI, BIYANG WEN, YINGWEI TIAN, (Member, IEEE), SIJIE WANG, AND YUKUN YIN

Radar and Signal Processing Laboratory, Electronic Information School, Wuhan University, Wuhan 430079, China

Corresponding author: Yingwei Tian (tianyw@whu.edu.cn)

This work was supported in part by the National Natural Science Foundation of China under Grant 61671331 and Grant 41706200, in part by the National Key Research and Development Program of China under Grant 2017YFC0405703, in part by the China Postdoctoral Science Foundation under Grant 2018T110799, and in part by the Fundamental Research Funds for the Central Universities under Grant 2042019kf1001.

ABSTRACT Monitoring small drones is significant for security requirements, but it is challenging because of small drones' low radar cross section (RCS) and hovering ability. In order to analyze the effect of radar waveform on the echo spectra and optimize the waveform design, an analytical expression of the rotor's temporal RCS is desired. Integral model, a widely used radar echo model of the rotor's temporal RCS, does not involve the electromagnetic scattering, thus it cannot be applied to all frequency bands. The method of moments (MoM) is a strictly numerical method based on the Maxwell's equations, but cannot obtain the analytical expression. Hence, this paper proposes a new method combing the integral model and MoM to model the rotor's temporal RCS in very high frequency (VHF) band. The linear frequency modulation (LFM) signal which has a high Doppler tolerance and a large gain bandwidth product is adopted in optimizing waveform parameters design. Based on the new method, the analytical expression of LFM echo is also derived. Moreover, the spectral spread over range and Doppler dimension caused by the rotating rotors is analyzed in detail. A criterion for optimizing the LFM waveform parameters for small drone detection is presented. Field experiments confirm the validity of the echo model and waveform parameters optimization criterion, and the full Acrylonitrile Butadiene Styrene small drone is successfully detected in VHF band. In addition, experiments are implemented to verify the applicability of the echo model and waveform parameters optimization method to other drones with different size.

INDEX TERMS Small drone detection, electromagnetic scattering, method of moments (MoM), numerical simulation, linear frequency modulation (LFM) signal.

I. INTRODUCTION

Recently, small drones or micro-Unmanned Air Vehicles (m-UAVs) have been widely used due to their low cost and easy operation, which give rise to the threat of security system [1], [2]. Technologies for detecting and tracking m-UAVs are desperately needed. One promising way is to employ the radar system. However, m-UAVs typically have the hovering ability, low radar cross section (RCS) and fly at low altitude, which make the monitoring of m-UAVs more difficult [3]. In order to examine and improve the capability of existing radar systems to meet these new challenges, the precise understanding about the radar echo characteristics of m-UAVs is required, especially the micro-Doppler signature generated by the rotating component [4], [5].

Integral model, a widely used radar echo model of rotor's temporal RCS, was proposed by Chen [6], but this echo model does not involve the electromagnetic scattering. Target signatures are inherent in echo amplitudes and phases dependent on the scatterer's dielectric properties, physical size, shape, and the incident electric field's wavelength and polarization pattern [7]. Hence, the integral model is not applicable to all frequency bands. However, the applicability of integral model has not been further studied. Previous

The associate editor coordinating the review of this manuscript and approving it for publication was Guido Lombardi.

 This work is licensed under a Creative Commons Attribution 4.0 License. For more information, see http://creativecommons.org/licenses/by/4.0/

studies on the electromagnetic scattering of m-UAVs were mainly focused on S band and above, and numerical simulation and measurement are two common methods [8]–[14]. In addition, it is feasible to monitor m-UAVs using VHF/UHV band under horizontal-horizontal polarization [15]. Therefore, the optimized radar waveform parameters design for drone detection based on m-UAVs echo modeling in VHF band is significant. In order to reduce the computational complexity, Pouliguen *et al.* [10] excluded the interactions between the airframe and the rotors. Schröder [14] numerically analyzed the time-frequency spectra of four rotating rotors, one rotating rotors and a full DJI Phantom Vision 2 assembled with four rotating rotors, respectively. The simulated time-frequency spectra indicated that the airframe only increased the contribution of zero-frequency component and multiple rotors resulted in the superposition of different initial rotation angles. The two contributions are basically independent of each other. The total calculation of a full m-UAV took 160 days.

The analytical expression of the rotor's temporal RCS is desired to analyze the effect of radar waveform on the echo spectra and optimize the waveform design. In this paper, the numerical simulations of temporal RCS and micro-Doppler signature are conducted based on the quasi-stationary approach [16], because the rotating rate is much slower than the speed of light and the angular rotation frequency is negligible compared with the radar frequency. Integral model does not involve the electromagnetic scattering, thus it cannot be applied to all frequency bands. The method of moments (MoM) is a rigorously numerical method based on the Maxwell's equations, but cannot obtain the analytical expression. Hence, a new method combing the integral model and MoM is proposed to model the rotor's temporal RCS in VHF band. The integral model is adjusted by the MoM through scaling factors to obtain a modified model. In order to reduce the computational cost, the modified model of a single rotor is used to represent that of a whole m-UAV in optimizing the radar waveform parameters design. Considering the low RCS of m-UAVs, the linear frequency modulation (LFM) signal which has a high Doppler tolerance and a large gain bandwidth product is adopted here. The analytical solution of LFM echo is derived based on the modified model. The waveform parameters design and optimization involving the LFM signal is investigated based on numerical simulation. In addition, the spectral spread in both range and Doppler dimension caused by the rotation and jitter of rotors is analyzed in detail. Finally, field experimental results are given to confirm the validity of the proposed echo model and waveform parameters optimization criterion.

This paper is organized as follows. The signal model is given in Section II. The radar waveform parameters design and optimization are proposed in Section III. Experimental results and analysis are shown in Section IV. Conclusions are drawn in Section V.

TABLE 1. Parameters of the integral model.

Symbol	Parameter	Specification
f_c	radar frequency	295 MHz
c	light speed	3×10^8 m/s
σ	scattering coefficient	1
L	blade length	122 mm
r_0	radial distance	100 m
f_{rot}	rotating speed	100 r/s (revolutions per seconds)
θ_0	initial rotation angle	0°
β	pitch angle	0°

Note: r_0 is the radial distance between radar and the center of rotor.

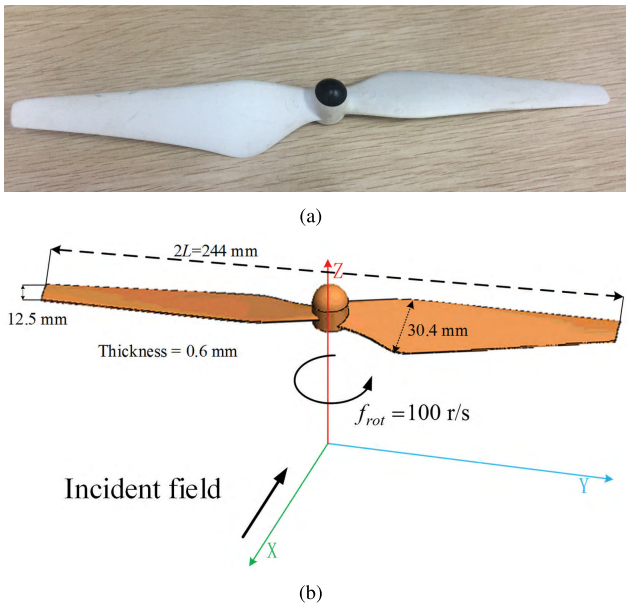

(a) (b)

FIGURE 1. (a) Photograph and (b) CAD model of a real rotor.

II. SIGNAL MODEL

A. THE DIFFERENCE BETWEEN MOM AND INTEGRAL MODEL

The radar baseband echo scattered by a single rotor (including two blades) incorporating a single frequency f_c signal source can be derived as [6]

$$s_{\text{inte}}(t) = 2\sigma L \exp(-j4\pi f_c r_0/c) \times \text{sinc}(4\pi L f_c \cos\beta \cos(\theta_0 + 2\pi f_{rot} t)/c) + n(t) \quad (1)$$

where $n(t)$ is the Gaussian White Noise (GWN), and the meanings and value of the remaining parameters are shown in Table 1. During the derivation, the two blades are assumed as the line segment with length of L, whose shape, width and material are ignored, and every point of the line segment is treated as an ideal scatterer with scattering coefficient σ. The pitch angle β between the signal source and rotor is set as 0° for simplicity. The detailed derivation of (1) can be found in [6].

MoM is a rigorous numerical method that is applicable to all frequencies, and it strictly satisfies the Maxwell's equations [17]. The DJI Phantom Vision 3 rotor model is investigated with MoM, as shown in Fig. 1. Two mainstream

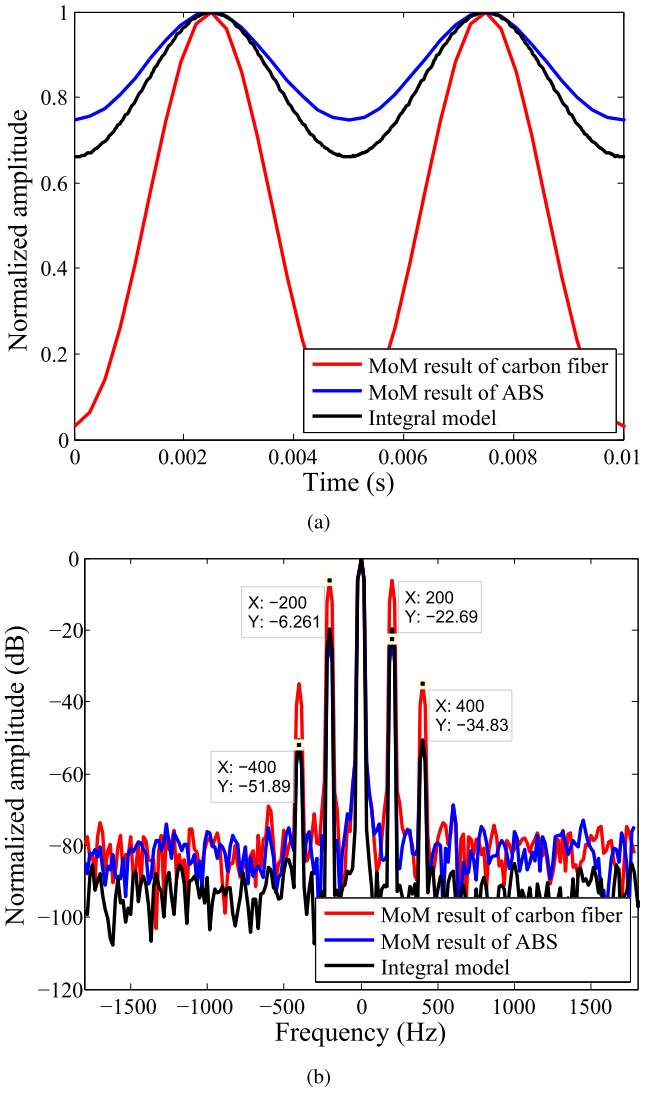

FIGURE 2. **(a) The temporal RCS and (b) Doppler spectra simulated using integral model and MoM, respectively.**

materials, Acrylonitrile Butadiene Styrene (ABS) and carbon fiber, are considered, respectively. The complex permittivity is defined as [18]

$$\varepsilon_{eff} = \varepsilon_r - j\sigma/\omega \tag{2}$$

where ε_r is the relative permittivity, σ is the conductivity, and ω denotes the radio wave angular frequency. The simulations assume that ε_r and σ of carbon fiber are equal to 50 and 6.25×10^4 S/m, respectively, and both ε_r and σ of ABS are equal to 2.8 and 10^{-15} S/m, respectively [8], [19]. The rotating speed is set as 100 r/s and the initial rotation angle is 0° (i.e., positive x-axis), and the positive angle corresponds to the counterclockwise direction. The Horizontal-Horizontal polarization is adopted and 295 MHz is selected as radar frequency.

The numerical simulations of temporal RCS and Doppler spectra are conducted based on the quasi-stationary approach [16]. Fig. 2 shows the simulated results using integral model and MoM, respectively, and the results are normalized by their respective maxima. As can be seen in Fig. 2(a), the temporal RCS distributions associated with two models have a similar shape. The peaks occur when the rotor is illuminated frontally and the valleys appear on side illumination, but the slopes are obviously different. Fig. 2(b) shows the simulated Doppler spectra with signal-to-noise ratio (SNR) of 60 dB. The Doppler peaks centered by the zero Doppler frequency can be clearly observed, which appear periodically at an interval of $2f_{rot}$ and their amplitudes decrease with the Doppler shift. However, there is a significant difference between the Doppler peaks' amplitude of integral model and MoM results, the maximum difference is about 15 dB.

The integral model treats every point of rotor as an ideal scatterer, which is closer to the situation of optical region, that is to say, the size of rotor is electrically large. However, in VHF band, the size of m-UAVs rotor is comparable or smaller than the radio wavelength, which may be the reason why significant differences between integral model and MoM occur.

B. MODIFIED MODEL INCORPORATING MOM RESULTS

To analyze the effect of radar waveform on the echo spectra and optimize the waveform design, an accurate analytical expression of the rotor's temporal RCS is desired. MoM is a strictly numerical method, but cannot obtain an analytical expression. Here, a new method combining the integral model and MoM is proposed, where the former is adjusted by the latter through scaling factors. In other words, the temporal RCS obtained by MoM is assumed to be the ground truth, and the results of integral model should be scaled to fit the ground truth. The correction function is obtained by fitting the scaling factors with several sine functions, as given by

$$CF(t) = \sum_{m=1}^{\infty}\sum_{i=1}^{I} a_i \sin[b_i \frac{f_{rot}}{100}(t + \frac{\theta_0}{2\pi f_{rot}}) + c_i] \times u_1(t - \frac{m}{f_{rot}} + \frac{\theta_0}{2\pi f_{rot}}) \tag{3}$$

where

$$u_1(t) = \begin{cases} 1, & 0 \le t < 1/f_{rot} \\ 0, & t > 1/f_{rot} \end{cases} \tag{4}$$

Thus, the modified model of the rotor's temporal RCS can be expressed as

$$s_{mod}(t) = CF(t) \times 2\sigma L \exp(-j4\pi f_c r_0/c) \times \mathrm{sinc}(4\pi L f_c \cos\beta \cos(\theta_0 + 2\pi f_{rot} t)/c) + n(t) \tag{5}$$

The reason why several sine functions are selected to fit the scaling factors is to facilitate the mathematical derivation of LFM echo in the process of stretch processing [20], which can be seen in SECTION III-A.

The modified model of two materials, carbon fiber and ABS, are investigated respectively. When the order of $CF(t)$,

i.e., the value of I, are set as 6 and 8 for carbon fiber and ABS, respectively, scaling factors of both materials can be well fitted by correction functions. The root mean squared error (RMSE) and adjusted R-square (R-sq) of carbon fiber material are equal to 2.97×10^{-4} and 1.0000, respectively. The RMSE and adjusted R-sq of ABS material are equal to 1.7×10^{-3} and 0.9987, respectively. The specific coefficients associated with the carbon fiber are given by

$$\begin{aligned}\mathbf{a}_{\mathbf{cb}} &= [1.133, 0.425, 0.7121, -0.1588, 0.1046, 0.0027]\\ \mathbf{b}_{\mathbf{cb}} &= [356.8, 1445, 608, 1946, 2236, 3513]\\ \mathbf{c}_{\mathbf{cb}} &= [-0.1997, -2.464, 1.695, 1.319, -0.1277,\\ &\quad -0.2433]\end{aligned} \tag{6}$$

and the coefficients for ABS are

$$\begin{aligned}\mathbf{a}_{\mathbf{ABS}} &= [3.767, 2.731, 0.09679, 0.01744, 0.01745,\\ &\quad 0.003856, 0.002702, 0.001474]\\ \mathbf{b}_{\mathbf{ABS}} &= [289, 352, 1232, 1943, 2373, 3011, 3663, 4354]\\ \mathbf{c}_{\mathbf{ABS}} &= [0.1279, 2.955, 1.651, 1.316, 2.313, 2.266,\\ &\quad 2.163, 1.85]\end{aligned} \tag{7}$$

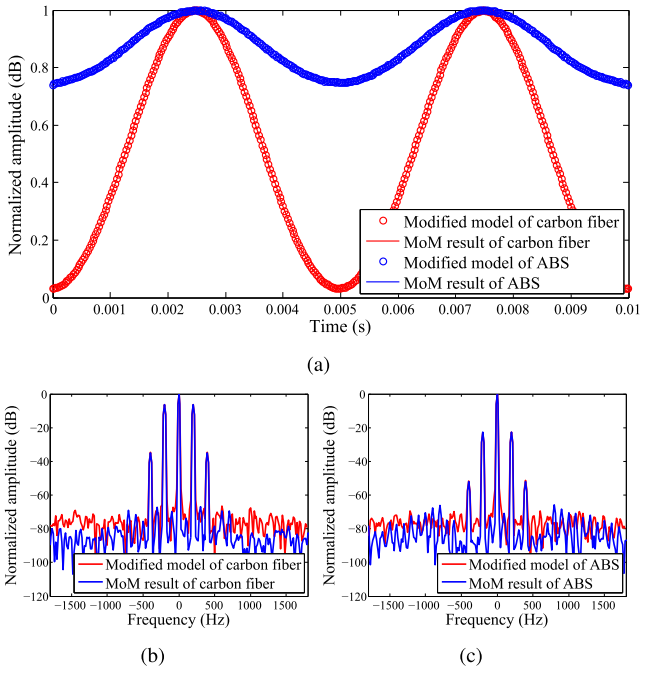

FIGURE 3. Comparison between the modified model and MoM. (a) The temporal RCS, and the simulated Doppler spectra for (b) carbon fiber rotor and (c) ABS rotor, respectively.

Fig. 3 shows the simulated results using the modified model and MoM, respectively, and the amplitudes are normalized by their respective maxima. As can be seen in Fig. 3(a), the temporal RCS distributions associated with two models are basically the same. Fig. 3(b) shows the simulated Doppler spectra with SNR of 60 dB. The amplitudes of Doppler peaks generated by the rotating rotor are basically the same. Comparing with the simulated results of integral model in Fig. 2, it is clearly that the modified model is more accurate and reliable. Thus, the modified model is adopted in the optimizing design of radar waveform parameters for small drone detection.

III. RADAR WAVEFORM PARAMETERS DESIGN AND OPTIMIZATION

A. LFM ECHO SIGNAL MODEL OF M-UAVS

Considering the low RCS of m-UAVs, the LFM signal which has a high Doppler tolerance and a large gain bandwidth product is adopted here. The above correction function $CF(t)$ is calculated at 295 MHz, but the LFM signal is a signal with a certain bandwidth. It is assumed that the scattering coefficient is basically constant in the narrow bandwidth of 10 MHz around 295 MHz. The (n + 1)-th transmitting LFM signal is defined as

$$s_{Tn}(t) = \cos[2\pi f_0 t + \pi k(t - nT_r)^2] \tag{8}$$

where f_0 is the start frequency, $k = B/T_r$ is the sweep slope, and B is the bandwidth, T_r is the frame time (sweep duration). For a single scattering point P on the rotor and the elevations of the signal source and rotor are set as the same, thus the echo of the (n+1)-th sweep can be calculated by the modified model as

$$s_{Rn\_p}(t) = \sigma CF(t)\cos[2\pi f_0(t - t_d) + \pi k(t - nT_r - t_d)^2] \tag{9}$$

where

$$t_d = 2R_p(t)/c \tag{10}$$

and

$$R_p(t) = r_0 + vt + x_i \cos\beta \cos(\theta_0 + 2\pi f_{rot} t) \tag{11}$$

v is the radial velocity of the translational movement, x_i is the distance from the scattering point P to the center of rotor, and the meanings of the remaining parameters are the same as (1).

The stretch processing [20] is a pulse compression technique and is typically used in radar modes. The echo of the (n + 1)-th sweep is stretched by multiplying it with a local oscillator LFM signal that has the same sweep rate as the transmitted signal. The stretched output is derived by using a time-domain approach. After removing $1/c^2$ and other constant items, the complex exponential expression of the basedband time-domain stretched output can be simplified as

$$\begin{aligned}&\tilde{s}_{Rn\_p}(t)\\ &= \frac{1}{2}\sigma CF(\mathrm{t})\\ &\quad \times \exp\left[j4\pi f_0 \frac{vt}{c} + 4\pi f_0 \frac{x_i \cos\beta \cos(\theta_0 + 2\pi f_{rot} t)}{c}\right]\\ &\quad \times \exp\left\{j4\pi k\left[\frac{r_0}{c} + \frac{vt}{c} + \frac{x_i \cos\beta \cos(\theta_0 + 2\pi f_{rot} t)}{c}\right]\right.\\ &\quad \left.\times (t - nT_r)\right\}\end{aligned} \tag{12}$$

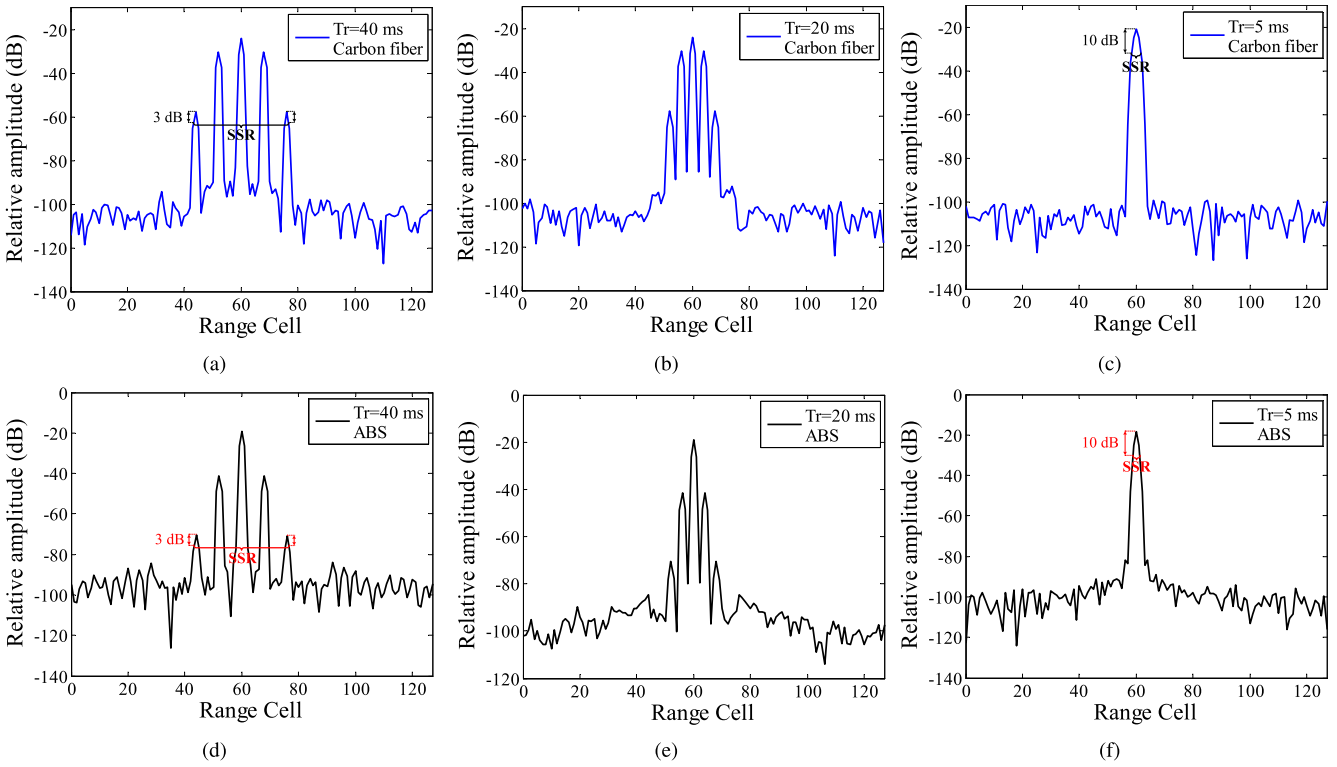

FIGURE 4. The simulated range spectra under different frame time for carbon fiber and ABS materials, respectively.

For the (n + 1)-th sweep signal, $t \in [nT_r, (n+1)T_r)$, therefore, $t' = t - nT_r \in [0, T_r)$, and the Doppler shift is $f_D = 2f_0 v/c$, so the expression of (12) can be rewritten as

$$\begin{aligned}
&\hat{s}_{Rn_p}(t') \\
&= \frac{1}{2}\sigma CF(t' + nT_r)\exp(2\pi f_D n T_r) \\
&\quad \times \exp\left[j2\pi\left(f_D + \frac{2kr_0}{c} + \frac{2kvt'}{c} + \frac{2kvnT_r}{c}\right)t'\right] \\
&\quad \times \exp\left\{j4\pi f_0 \frac{x_i \cos\beta \cos[\theta_0 + 2\pi f_{rot}(t' + nT_r)]}{c}\right\} \\
&\quad \times \exp\left\{j4\pi k \frac{x_i \cos\beta \cos[\theta_0 + 2\pi f_{rot}(t' + nT_r)]}{c} t'\right\} \quad (13)
\end{aligned}$$

By integrating (13) over the length 2L of the rotor, the (n + 1)-th received signal becomes

$$\begin{aligned}
s_{Rn}(t') &= \int_{-L}^{L} \hat{s}_{Rn_p}(t')dx_i \\
&= \sigma LCF(t' + nT_r)\exp(2\pi f_D n T_r) \\
&\quad \times \exp\left\{j2\pi\left[f_D + \frac{2kr_0}{c} + \frac{2kvt'}{c} + \frac{2kvnT_r}{c}\right]t'\right\} \\
&\quad \times \operatorname{sinc}\left\{\begin{array}{l}\dfrac{4\pi f_0 L \cos\beta \cos[\theta_0 + 2\pi f_{rot}(t' + nT_r)]}{c} \\ + \dfrac{4\pi kL \cos\beta \cos[\theta_0 + 2\pi f_{rot}(t' + nT_r)]t'}{c}\end{array}\right\} \\
&\quad (14)
\end{aligned}$$

As can be seen in (14), the echo model consists of four parts, the correction function $CF(\cdot)$, the contribution of sweep number $\exp[2\pi f_D n T_r]$, the translational component $\exp\{j2\pi[f_D + 2kr_0/c + 2kvt'/c + 2kvnT_r/c]t'\}$ and the modulation of rotating rotor $\operatorname{sinc}(\cdot)$. The echo signal is modulated by the rotating rotor through the sinc function $\operatorname{sinc}(\cdot)$, and this modulation affects both the range and Doppler information of the m-UAV target in the radar range-Doppler (RD) spectra. In the optimization of radar waveform parameters, this echo model of a single rotor (14) is used to represent that of a whole m-UAV. Based on this echo model, the numerical simulations are implemented to analyze the effects of rotating motion associated with different waveform parameters.

B. SPECTRAL SPREAD IN RANGE DIMENSION

The parameters for range spectra simulation are listed in Table 2. The simulated range spectra under different frame time for carbon fiber and ABS materials, respectively, are

TABLE 2. Parameters configuration for simulation.

Symbol	Parameter	Specification
f_0	start frequency of LFM signal	290 MHz
B	bandwidth	10 MHz
T_r	frame time	40/20/5 ms
r_0	radial distance	900 m
v	radial velocity	0 m/s
f_{rot}	rotating speed	100 r/s

Note: the other parameters not given here are set the same as listed in Table 1.

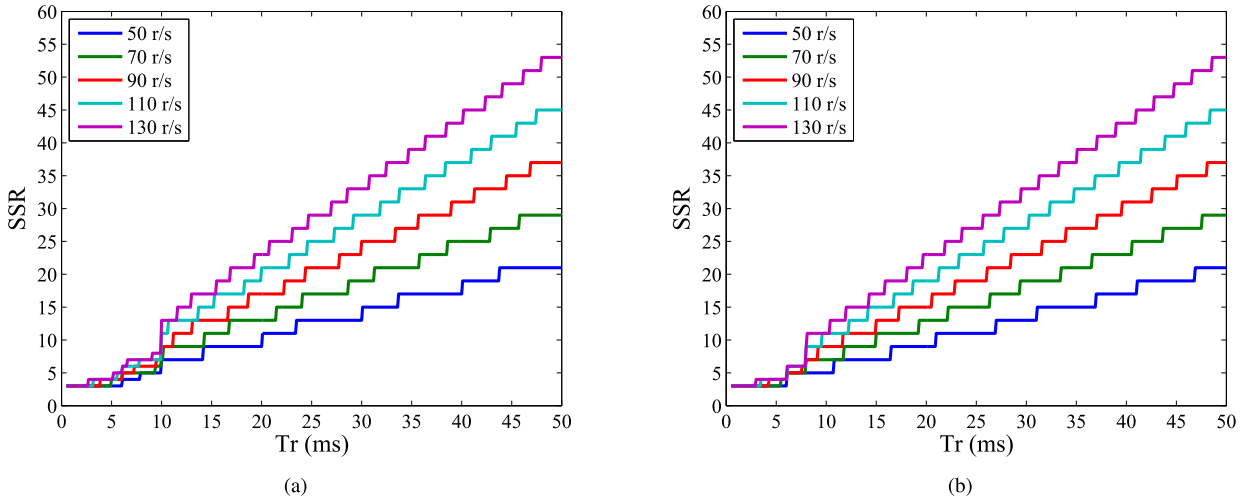

FIGURE 5. The simulated SSR distribution under different T_r and f_{rot} for (a) carbon fiber and (b) ABS materials, respectively.

shown in Fig. 4. As can be seen in Fig. 4 (a) and Fig. 4(d) at $T_r = 40$ ms, the modulated peaks appear periodically at a frequency interval of $2f_{rot}$ around the 60-th range cell which corresponds to the distance from the rotor to radar, and the amplitudes of these peaks decrease rapidly as the range cell shift increases. The results of carbon fiber and ABS materials show the same trend, except that the amplitudes of the modulated peaks have different decreasing rate. These modulated peaks will lead to false target detection. Moreover, the diffusion of energy will make the detection of m-UAVs more difficult. Therefore, it is necessary to solve the diffusion of energy in range dimension.

It is feasible to address this problem by redesigning the waveform parameters. The interval of these modulated peaks depends only on the rotation frequency of the rotor rather than the number of range cell. According to the principle of stretch processing, the range resolution is $\Delta r = c/2B$, and the corresponding frequency spacing in the range spectrum is $\Delta f = 1/T_r$. Thus, as can be seen in Fig.4 from $T_r = 40$ ms to $T_r = 5$ ms, these modulated peaks are gradually merged into one range cell (60-th range cell). When T_r decreases from 40 ms to 5 ms, the pulse compression gain also decreases, but the energy is concentrated on a single peak. Hence, the amplitudes of the 60-th range cell at $T_r = 5$ ms and at $T_r = 40$ ms are comparable.

As can be seen in Fig.4 (a) and Fig. 4(d), when several modulated peaks occur, the spectral spread in range dimension (SSR) is defined as the number of range cells from the first peak's 3 dB point to the last peak's 3 dB point. When the modulated peaks are merged into one peak in Fig.4 (c) and Fig. 4(f), the spectral spread in range dimension SSR is defined as the number of range cells corresponding to the peak's width of 10 dB. The SSR under different T_r and f_{rot} are investigated for both materials, respectively, to determine the optimal T_r. Considering that the rotating speed f_{rot} of four-rotor m-UAVs is mostly lower than 130 r/s [21], and the rotation speed of six/eight-rotor m-UAVs is even lower [22], thus the speeds within 50-130 r/s are taken into account. Fig. 5 shows the simulated SSR distribution under different T_r and f_{rot} for carbon fiber and ABS materials, respectively. As can be seen in Fig. 5, reducing T_r can effectively decrease SSR. Considering that the leakage of spectrum caused by windowing and the 'Picket Fence Effect' caused by discrete Fourier transform will widen the main lobe, the spectral spread of SSR $= 4$ is acceptable, and the corresponding T_r is 5 ms for both materials.

Moreover, further reducing T_r will decrease pulse compression gain. Therefore, to make a compromise between the spectral spread in range dimension and pulse compression gain, an optimized parameter of frame time T_r is 5 ms.

C. SPECTRAL SPREAD IN DOPPLER DIMENSION

Considering the low RCS of m-UAVs, coherent integration is often implemented to enhance the SNR of target echo. Thus, Barrick's method [23] is adopted to obtain the RD spectrum.

Simulations assume that f_{rot} and coherent integration sweep numbers (CIN) are 110 r/s and 256, respectively, and the SNR before pulse compression is 20 dB. The other parameters are the same as listed in Table 1 and Table 2. The simulated RD spectra using carbon fiber material under different frame time ($T_r \leq 5$ ms) are shown in Fig. 6, the spectral spread in range dimension has been greatly suppressed. In addition, in Fig. 6(a) at $T_r = 1$ ms, the Doppler peaks centered by the zero Doppler frequency can be clearly observed along Doppler dimension, which appear periodically at frequency interval of $2f_{rot}$ and their amplitudes decrease with the Doppler shift. In Fig. 6(b), these peaks are under-sampled when $T_r = 5$ ms. The rotating speed f_{rot} can be retrieved by the non-aliasing sampling of the first pair of Doppler peaks in RD spectrum [15].

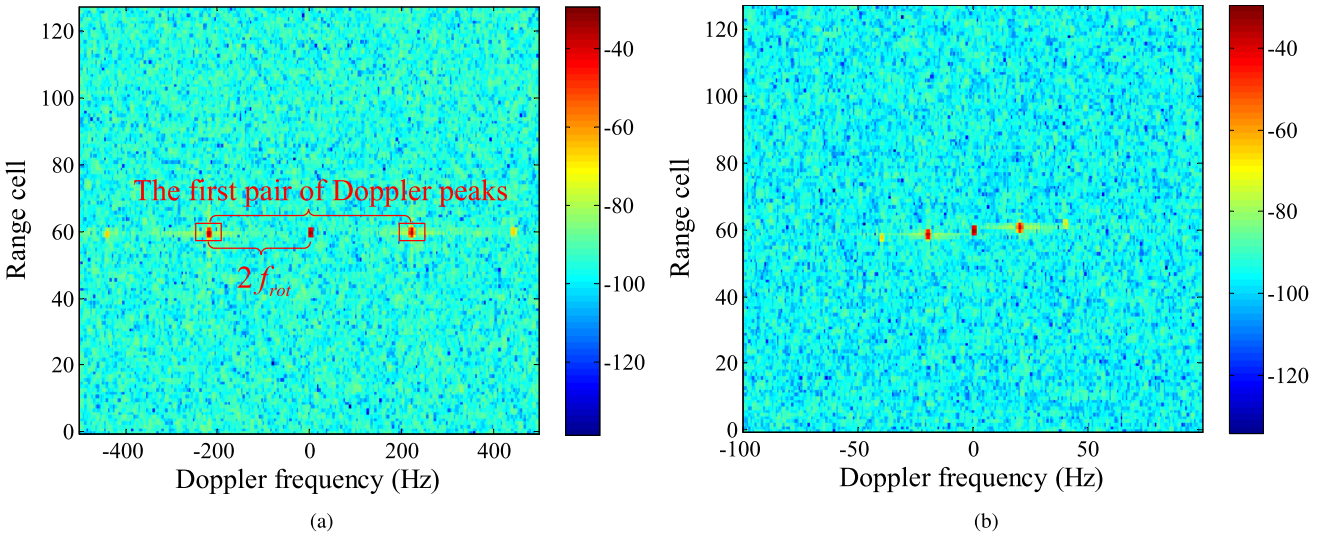

FIGURE 6. The simulated RD spectra for carbon fiber at (a) $T_r = 1$ ms and (b) $T_r = 5$ ms.

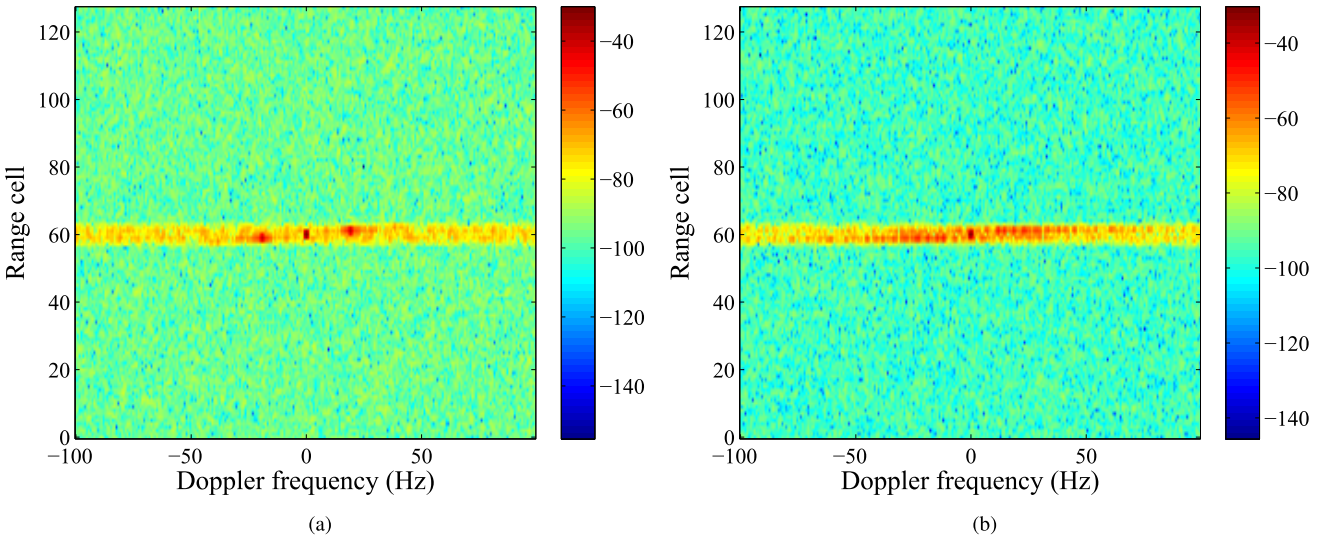

FIGURE 7. The simulated RD spectra for carbon fiber at (a) $\alpha = 1\%$ and (b) $\alpha = 10\%$.

But in practice, in order to counter the wind and maintain a stable posture, it is impossible for m-UAVs to maintain a steady rotating speed for a long time. The frequencies of these Doppler peaks will accordingly change with the rotation speed. Hence, simulations assume that the rotating speed fluctuates every 5 ms. The jitter rate $\alpha = \Delta\bar{f}_{rot}/f_{rot}$ is defined as the ratio of the average speed variation $\Delta\bar{f}_{rot}$ to the rotating speed. The rotating speed is set as $f_{rot} = 110$ r/s. Carbon fiber material is analyzed here, and CIN is 256, $T_r = 5$ ms, and the cases of $\alpha = 1\%$ and $\alpha = 10\%$ are studied, respectively.

As can be seen in Fig. 7, when the jitter of rotating speed occurs, these Doppler peaks spread significantly in Doppler dimension. As the jitter increases from $\alpha = 1\%$ to $\alpha = 10\%$, these Doppler peaks are spread over the entire Doppler axis. The spectral spread in Doppler dimension is significantly related to the degree of jitter, which is difficult to predict in practice. Therefore, it may be infeasible to obtain the rotating speed form the RD spectrum. The cases associated with ABS material and different fluctuating interval of rotating speed draw the similar conclusion, which are not repeated here.

D. ANALYSIS AND PARAMETERS DESIGN OF LFM SIGNAL FOR M-UAVS DETECTION

The spectral spread in both range and Doppler dimensions occur periodically at the frequency interval of $2f_{rot}$. The spectral spread in range dimension can be solved by decreasing T_r, but at the same time, the pulse compression gain also decreases. Thus, coherent integration is implemented to improve the performance of detecting m-UAVs. The Doppler resolution is $\Delta f_{Dop} = 1/(\text{CIN} \cdot T_r) = 1/\text{CIT}$, where CIT is

the coherent integration time. The spectral spread in Doppler dimension can also be solved by decreasing CIT, but it is unpractical and unnecessary. On the one hand, the decrease of CIT makes it more difficult to detect m-UAVs, especially the full ABS m-UAVs, whose dielectric properties are close to air. On the other hand, the characteristics of spectral spread in Doppler dimension provides additional information for m-UAVs recognition complementary to existing recognition methods. What's more, the spectral spread in Doppler dimension is the significant information which can be used to detect the hovering m-UAVs.

From the above simulations and analysis above, an optimized parameter of frame time T_r is 5 ms. Moreover, the following issues should also be considered when designing the LFM parameters for m-UAVs detection.

1) The LFM signal exists range-Doppler coupling [24], and stretch processing is a method of mismatched filter. The Doppler shift f_D caused by radial velocity of m-UAVs will lead to a deviation in the range cell estimate. To avoid the deviation over one range cell, f_D should be less than $1/T_r$, which means

$$T_r < 1/f_D = 1/(2f_0 v/c) \tag{15}$$

2) To avoid Doppler aliasing, the Doppler sampling rate $f_{s\_Dop} = 1/T_r$ should be greater than $2f_D$, i.e.

$$T_r < 1/2f_D = 1/(4f_0 v/c) \tag{16}$$

It is clearly that the constraint of (16) is stricter than that of (15).

3) In order to avoid the spread in range dimension caused by the radial displacement of m-UAVs during the coherent integration time, the radial displacement $CIT \cdot v$ should be less than the range resolution $\Delta r = c/2B$. CIT should fulfil the following equation

$$\mathrm{CIT} = \mathrm{CIN} \cdot T_r < \frac{c}{2Bv} \tag{17}$$

Considering that the maximum radial velocity v of m-UAVs is about 20 m/s [21], [22], the calculated T_r from (16) should be less than 12.9 ms. Therefore, $T_r = 5$ ms is still applicable. When T_r and B are set as 5 ms and 10 MHz, respectively. The calculated CIT and CIN from (17) should be less than 750 ms and 150, respectively. This paper focuses on the modulation of micro-Doppler, so the radial velocity of m-UAVs for simulations is set as 0, thus the CIN is not strictly limited to be less than 150.

IV. EXPERIMENTAL RESULTS AND ANALYSIS

Field experiments are implemented to verify the correctness of the proposed echo model and the validity of waveform parameter design. The DJI phantom 3 m-UAV assembled with either carbon fiber or ABS material rotors is fixed on the ground, and the experimental scenario is shown in Fig. 8. The radar system employs the LFM signal, and the specifications are listed in Table 3. Considering that the RCS of ABS is much lower than that of carbon fiber, the CIN of ABS material is increased to 1024. According to Barrick's method, the received signals are successively processed by stretch processing and coherent integration to obtain the RD spectra.

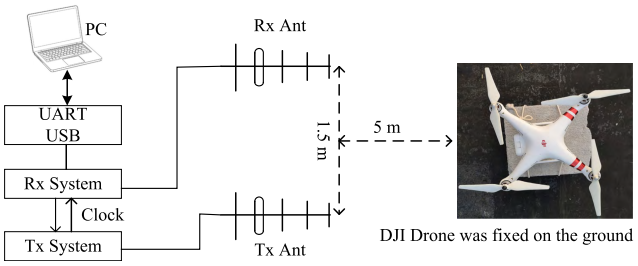

FIGURE 8. The experimental scenario for detecting a quadcopter.

TABLE 3. Radar specification.

Item	Specification
start frequency of LFM signal	290 MHz
bandwidth	10 MHz
frame time	40/5 ms
CIN	256 (carbon fiber), 1024 (ABS)
peak power	-10 dBm
antenna	Yagi-Uda antenna
polarization pattern	horizontal-horizontal polarization

A. CARBON FIBER MATERIAL

Four sets of data are collected when rotors are either at rest or rotating under different T_r. In order to clearly observe the spectral spread in range dimension, system delay is added during the experiments using the quadcopter for both materials. The RD spectrum measured when the rotors are stationary is shown in Fig. 9(a), and the distance of the m-UAV corresponds to the 55-th range cell due to the system delay. Since the direct path signal is much stronger than the scattered echo, in Fig. 9(b-d) and the other measured RD spectra, the region around the zero Doppler frequency has been excluded from the spectra to provide a clearer display of the micro-Doppler effect.

Fig. 9(b) shows the RD spectrum at $T_r = 40$ ms when the rotors rotate. As can be seen, the spectral spread in range dimension is more than 15 range cells. And the spectral spread in Doppler dimension is pretty serious, the Doppler peaks are spread over the entire Doppler axis. Fig. 9(c) and Fig. 9(d) are the RD spectra at $T_r = 5$ ms with different jitters of rotating speed. As can be seen, when T_r is reduced to 5 ms, the spectral spread in range dimension have been greatly suppressed, and the echo power is concentrated within the correct range cells, so the radial distance of m-UAV can be easily estimated from RD spectrum. The leakage of spectrum and the 'Picket Fence Effect' will widen the main lobe, thus the echo power cannot be concentrated in a single range cell.

The jitter rate α and fluctuating interval of the rotating speed are random and difficult to predict. During the experiment, most of measured results are similar to Fig. 9(d) whose Doppler peaks are spread over the entire Doppler axis and these peaks cannot be observed in Doppler dimension. Only

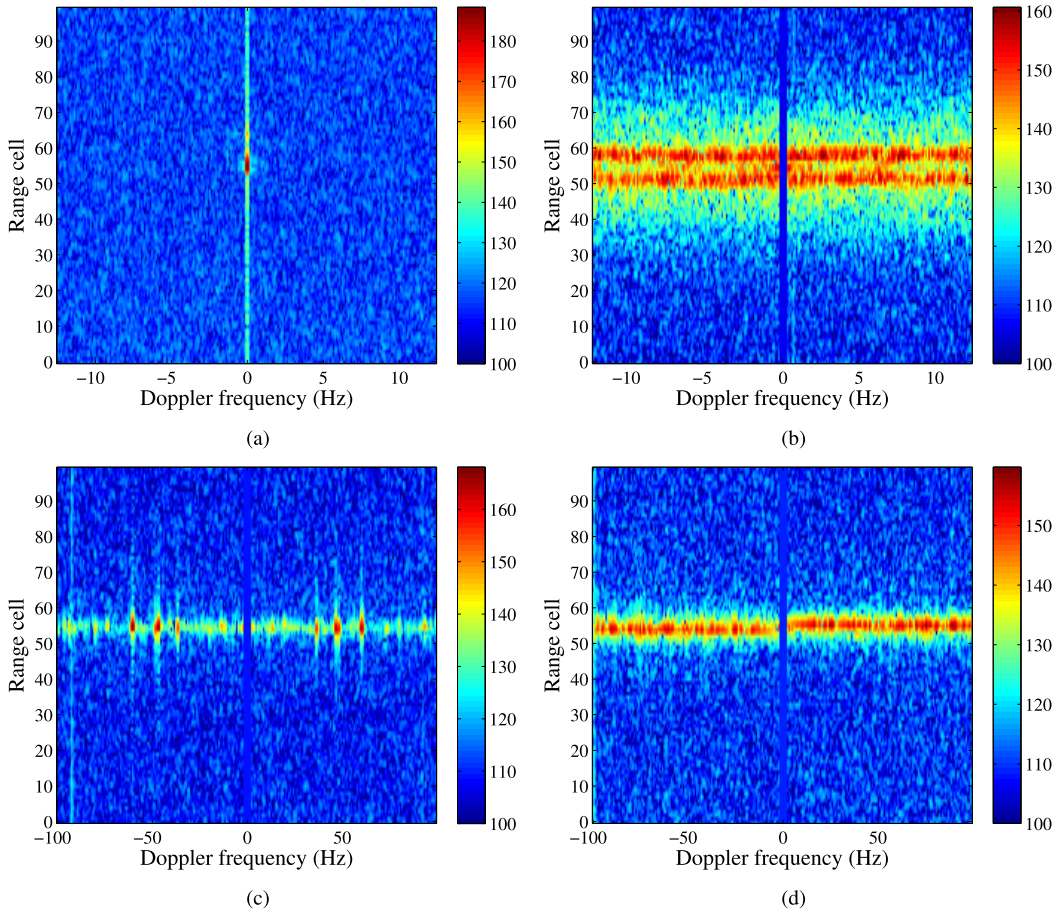

FIGURE 9. The measured RD spectra of m-UAV assembled with four carbon fiber rotors when (a) rotors stopping, $T_r = 40$ ms (b) rotors rotating, $T_r = 40$ ms, (c) rotors rotating, $T_r = 5$ ms and (d) rotors rotating with intensified jitter, $T_r = 5$ ms.

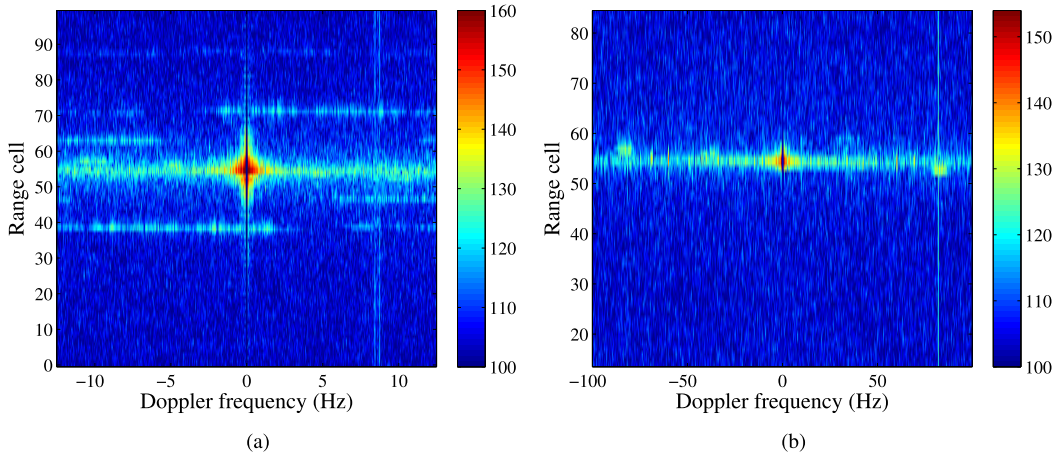

FIGURE 10. The measured RD spectra of m-UAV assembled with four ABS rotors at (a) $T_r = 40$ ms and (b) $T_r = 5$ ms.

a few results like Fig.9 (c) are measured whose Doppler peaks can be observed in Doppler dimension. Nevertheless, the spectral spread over Doppler axis due to the random jitter of rotation speed still remains. Considering the practical flying scene of m-UAVs, the jitter of rotating speed will be greater than that of the experimental scene. The spectral spread in Doppler dimension can be applied to recognize the m-UAVs with rotors and detect drones hovering in situ. The measured results are consistent with the simulations in SECTION III-C.

FIGURE 11. The DJI Matrice 600 Pro drone.

B. ABS MATERIAL

Fig. 10(a) shows the RD spectrum associated with the rotating ABS rotors for $T_r = 40$ ms. As can be seen, the spectral spread in both range and Doppler dimension is serious. In Fig. 10(b) at $T_r = 5$ ms, the spectral spread in range dimension has been greatly suppressed, and the echo power is concentrated within the target range cells. The measured RD spectra of carbon fiber and ABS materials are similar, but the echo power of ABS is much weaker than that of carbon fiber.

C. SIX-ROTORS M-UAVS

In order to further verify whether the optimized design of waveform parameter in this paper is applicable to other m-UAVs with different size, a DJI Matrice 600 Pro platform [22] assembled with six carbon fiber rotors is measured. The DJI Matrice 600 Pro shown in Fig. 11, is basically hovering in situ during the experiment. The radial distance from radar to drone is about 150 m. The CIN employs 256 and the radar specifications listed in Table 3 are used.

The RD spectrum at $T_r = 40$ ms is shown in Fig. 12(a). The spectral spread in range dimension is more than 15 range cells, and the spectral spread in Doppler dimension is even more serious, these Doppler peaks are spread over the entire Doppler axis. As can be seen in Fig. 12(b), when T_r is reduced to 5 ms, the spectral spread in range dimension have been greatly suppressed and the echo power is concentrated with the target range cells. The measured RD spectra are similar to the results of a DJI phantom 3 assembled with four carbon fiber rotors in Fig. 9. But the scattered echo of $T_r = 5$ ms is weaker than that of $T_r = 40$ ms, which may be caused by the size of Matrice 600 Pro. That is to say, the effect of reducing CIT on echo power of the Matrice 600 Pro is greater than that of the DJI phantom 3. But the RCS and size of the Matrice 600 Pro are larger than those of the DJI phantom 3, which makes the echo power of the former greater than that of the latter under the same test condition. Experimental results confirm that the optimized design of waveform parameter is still applicable to other m-UAVs with different size in VHF band.

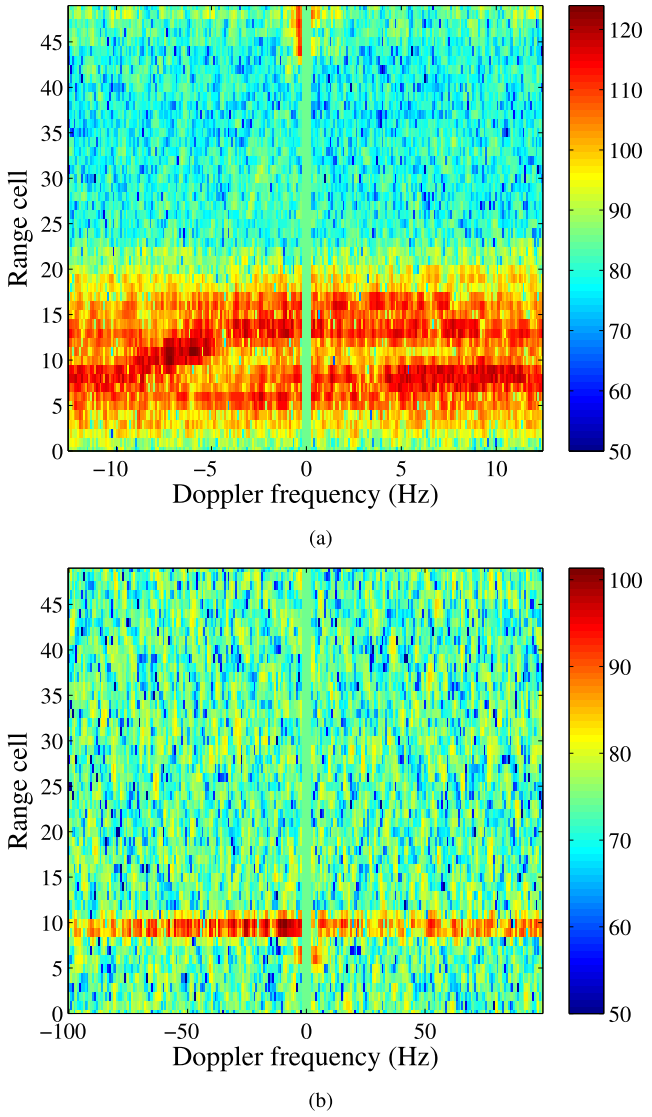

FIGURE 12. The measured RD spectra of the DJI Matrice 600 Pro at (a) $T_r = 40$ ms and (b) $T_r = 5$ ms.

V. CONCLUSION

In order to examine and improve the capability of existing radar systems to meet the challenge of monitoring m-UAVs, this paper presents an optimized radar waveform parameter design for m-UAVs detection based on echo modeling and experimental analysis. The modified radar echo model of m-UAV rotor's temporal RCS is proposed based on the MoM in VHF band. Based on the modified model, the analytical expression of LFM echo is derived and adopted in optimizing waveform parameters design. The spectral spread in both range and Doppler dimension caused by the rotation and jitter of rotors is analyzed in detail. The spectral spread in range dimension leads to false target detection and the diffusion of energy makes the detection of m-UAVs more difficulty. To make a compromise between the spectral spread in range dimension and the pulse compression gain, a heuristic parameter of frame time is found to be 5 ms. In addition, coherent

integration is implemented to enhance the echo power. The spectral spread in Doppler dimension can also be removed by decreasing CIT, but it is unpractical and unnecessary. Reducing CIT will make the detection of m-UAVs more difficult, particularly the full ABS m-UAVs. Additionally, the spectral spread in Doppler dimension can be applied to recognize the m-UAVs with rotors and detect drones hovering in situ. In addition, a criterion for optimizing the LFM waveform parameters for small drone detection is proposed, when the radial velocity v of m-UAVs is taken into account. Experiments confirm the validity of the echo model and the criterion of waveform parameters design, and successfully detect the full ABS m-UAVs in VHF band. Moreover, the experiments employed the platform of DJI Matrice 600 Pro, verify that the waveform design criterion and echo model are still applicable to other m-UAVs with different size.

In addition, several aspects need to be further studied.

1) The spread in Doppler dimension will interferes the estimation of radial velocity v, when the strong backscattering of airframe has been taken into account.

2) The spread in Doppler dimension also impairs the target detection when multiple m-UAVs have a close radial distance.

3) The classical target detection algorithm (such as constant false alarm [3]) cannot be directly used, because the scattered echo of m-UAVs is no longer a point target in RD spectrum.

Based on the credible radar echo model proposed in this paper, it is feasible but challenging to solve the above issues by appropriate algorithm, which need to be completed in the future. Moreover, the pseudo-random code phase modulation (PCPM) signal has no range-Doppler coupling, which means no spectral spread in range dimension caused by micro-Doppler. But the low Doppler tolerance of PCPM signal makes it disadvantageous to detect target with a high velocity. The performance of PCPM signal for UAV detection is also worth studying in the future.

REFERENCES

[1] H. Borrion, "What is the buzz about drone crime? Honeypots, sting operations and other uplifting discussion topics," in *Proc. Stockholm Criminol. Symp.*, 2015, p. 98.

[2] M. Ritchie, F. Fioranelli, and H. Borrion, "Micro UAV crime prevention: Can we help Princess Leia?" in *Crime Prevention in the 21st Century*. Cham, Switzerland: Springer, 2017, pp. 359–376.

[3] J. Eaves and E. Reedy, *Principles of Modern Radar*. Berlin, Germany: Springer, 2012.

[4] V. C. Chen, "Analysis of radar micro-Doppler with time-frequency transform," in *Proc. 10th IEEE Workshop Stat. Signal Array Process.*, Aug. 2000, pp. 463–466.

[5] V. C. Chen, F. Li, S.-S. Ho, and H. Wechsler, "Micro-Doppler effect in radar: Phenomenon, model, and simulation study," *IEEE Trans. Aerosp. Electron. Syst.*, vol. 42, no. 1, pp. 2–21, Jan. 2006.

[6] V. C. Chen, *The Micro-Doppler Effect in Radar*. Norwood, MA, USA: Artech House, 2011.

[7] B. Torvik, K. E. Olsen, and H. Griffiths, "Classification of birds and UAVs based on radar polarimetry," *IEEE Geosci. Remote Sens. Lett.*, vol. 13, no. 9, pp. 1305–1309, Sep. 2016.

[8] A. Schroder, M. Renker, U. Aulenbacher, A. Murk, U. Boniger, R. Oechslin, and P. Wellig, "Numerical and experimental radar cross section analysis of the quadrocopter DJI phantom 2," in *Proc. IEEE Radar Conf.*, Oct. 2015, pp. 463–468.

[9] M. Ritchie, F. Fioranelli, H. Griffiths, and B. Torvik, "Micro-drone RCS analysis," in *Proc. IEEE Radar Conf.*, Oct. 2015, pp. 452–456.

[10] P. Pouliguen, L. Lucas, F. Müller, S. Quete, and C. Terret, "Calculation and analysis of electromagnetic scattering by helicopter rotating blades," *IEEE Trans. Antennas Propag.*, vol. 50, no. 10, pp. 1396–1408, Oct. 2002.

[11] A. Herschfelt, C. R. Birtcher, R. M. Gutierrez, Y. Rong, H. Yu, C. A. Balanis, and D. W. Bliss, "Consumer-grade drone radar cross-section and micro-Doppler phenomenology," in *Proc. IEEE Radar Conf.*, May 2017, pp. 981–985.

[12] B. K. Kim, H.-S. Kang, and S.-O. Park, "Experimental analysis of small drone polarimetry based on micro-Doppler signature," *IEEE Geosci. Remote Sens. Lett.*, vol. 14, no. 10, pp. 1670–1674, Oct. 2017.

[13] M. Jian, Z. Lu, and V. C. Chen, "Experimental study on radar micro-Doppler signatures of unmanned aerial vehicles," in *Proc. IEEE Radar Conf.*, May 2017, pp. 854–857.

[14] A. Schröder, U. Aulenbacher, M. Renker, U. Böniger, R. Oechslin, A. Murk, and P. Wellig, "Numerical RCS and micro-Doppler investigations of a consumer UAV," *Proc. SPIE*, vol. 9997, Oct. 2016, Art. no. 999704.

[15] T. Li, B. Wen, Y. Tian, Z. Li, and S. Wang, "Numerical simulation and experimental analysis of small drone rotor blade polarimetry based on RCS and micro-Doppler signature," *IEEE Antennas Wireless Propag. Lett.*, vol. 18, no. 1, pp. 187–191, Jan. 2019.

[16] J. V. Bladel, "Electromagnetic fields in the presence of rotating bodies," *Proc. IEEE*, vol. 64, no. 3, pp. 301–318, Mar. 1976.

[17] R. F. Harrington, "Matrix methods for field problems," *Proc. IEEE*, vol. 55, no. 2, pp. 136–149, Feb. 1967.

[18] J. Baker-Jarvis, "Measuring the permittivity and permeability of lossy materials: Solids, liquids, metals, building materials, and negative index materials," U.S. Dept. Commerce, Nat. Inst. Standards Technol., Gaithersburg, MD, USA, Tech. Rep. NIST TN-1536, 2005.

[19] J. E. Atwater and R. R. Wheeler, Jr., "Complex permittivities and dielectric relaxation of granular activated carbons at microwave frequencies between 0.2 and 26 GHz," *Carbon*, vol. 41, no. 9, pp. 1801–1807, 2003.

[20] W. J. Caputi, "Stretch: A time-transformation technique," *IEEE Trans. Aerosp. Electron. Syst.*, vol. AES-7, no. 2, pp. 269–278, Mar. 1971.

[21] (2017). *The DJI Phantom 3 User Manual v1.0*. [Online]. Available: https://dl.djicdn.com/downloads/phantom_3/User%20Manual/Phantom_3_SE_User_Manual_v1.0_en.pdf

[22] (2018). *The DJI M600 Pro User Manual v1.0*. [Online]. Available: https://dl.djicdn.com/downloads/m600%20pro/20180417/Matrice_600_Pro_User_Manual_v1.0_EN.pdf

[23] D. E. Barrick, "FM/CW radar signals and digital processing," Wave Propag. Lab, Nat. Ocean. Atmos. Admin., Boulder, CO, USA, Tech. Rep. NOAA-TR-ERL-283-WPL-26, 1973.

[24] J. R. Klauder, A. C. Price, S. Darlington, and W. J. Albersheim, "The theory and design of chirp radars," *Bell Syst. Tech. J.*, vol. 39, no. 4, pp. 745–808, 1960.

TENGMINGYANG LI was born in Chongqing, China, in 1995. He received the B.Eng. degree from Wuhan University, Wuhan, China, in 2017, where he is currently pursuing the Ph.D. degree.

His current research interests include target tracking, electromagnetic scattering, and radar signal processing.

BIYANG WEN was born in Xiantao, Hubei, China, in 1963. He received the B.Eng. degree from Shanghai Jiao Tong University, Shanghai, China, in 1983, and the M.S. and Ph.D. degrees from Wuhan University, Wuhan, China, in 1990 and 1997, respectively.

Since 1990, he has been with the School of Electronic Information, Wuhan University, where he is currently a Professor. His current research interests include radio wave propagation and remote sensing of the ocean surface via high-frequency ground wave radar and UHF radar.

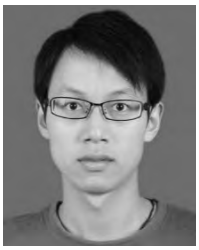

YINGWEI TIAN was born in Qianjiang, Hubei, China, in 1989. He received the B.Eng. and Ph.D. degrees from Wuhan University, Wuhan, China, in 2010 and 2015, respectively.

From 2015 to 2018, he was a Postdoctoral Fellow in geophysics with Wuhan University, where he is currently an Associate Researcher. His current research interests include ocean surface remote sensing via high-frequency ground wave radar and radar signal processing.

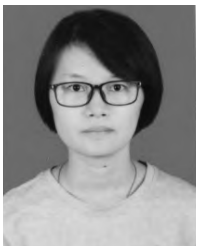

SIJIE WANG was born in Jian, Jiangxi, China, in 1995. She received the B.Eng. degree from Wuhan University, Wuhan, China, in 2016, where she is currently pursuing the Ph.D. degree.

Her current research interests include target tracking and information fusion.

YUKUN YIN was born in Xinyang, Henan, China, in 1997. He received the B.Eng. degree from Wuhan University, Wuhan, China, in 2018, where he is currently pursuing the Ph.D. degree.

His current research interests include electromagnetic scattering andoceanlike rough surface scattering via UHF radar.